Research Article

Abdullah R. Alzahrani*

A study of the anticancer potential of Pluronic F-127 encapsulated Fe_2O_3 nanoparticles derived from *Berberis vulgaris* extract

https://doi.org/10.1515/gps-2023-0126
received July 13, 2023; accepted October 9, 2023

Abstract: The study synthesized Pluronic F-127 nanoparticles that encapsulate Fe_2O_3 (PF127Fe_2O_3NPs), nanoparticles, characterized their formation, and evaluated their cytotoxicity and anticancer activity using *Berberis vulgaris* leaf extract, using various analytical methods such as FTIR, Ultraviolet-visible, photoluminescence, dynamic light scattering, X-ray diffraction, and morphology analysis. We assessed the antioxidant properties of PF127Fe_2O_3NPs, cytotoxicity, and apoptosis through 3-[4,5-dimethylthiazol-2-yl]-2,5 diphenyl tetrazolium bromide (MTT) assay and acridine orange/ethidium bromide staining in breast cancer cells, such as MCF7, and MDA-MB-231. The characterization results demonstrated that PF-127 was coated with Fe_2O_3 nanoparticles. MTT assay data revealed that PF127Fe_2O_3NPs effectively prevent cancer cells from proliferating and act as an anticancer drug. The antimicrobial results revealed that the fabricated nanoparticles are effective against gram-negative (*Klebsiella pneumoniae*, *Escherichia coli*, and *Shigella dysenteriae*) and gram-positive (*Streptococcus pneumoniae*, *Staphylococcus aureus*, and *Bacillus subtilis*) bacteria. Treatment of PF127Fe_2O_3NPs in a dose-dependent manner on MCF7, and MDA-MB-231, exhibited increased antioxidant activity, nuclear damage, and apoptotic activity. These results confirm the apoptotic activity of PF127Fe_2O_3NPs. The study concludes that MCF7 appears to be more sensitive to PF127Fe_2O_3NPs than MDA-MB-231. In conclusion, we have found that it can be used as an effective antioxidant and anticancer agent in therapeutics.

Keywords: Pluronic F-127-coated Fe_2O_3 nanoparticles, anticancer, MCF7, MDA-MB-231

1 Introduction

As an alternative to their enormous materials, nanoparticles are now being studied for a varied diversity of reasons and have enhanced biological activity due to their small size, high surface-to-volume ratio, and ability to change size and shape [1]. Nanoparticles are currently made using several physicochemical techniques for various applications, such as biological sensors, solar cells, agriculture, and textiles [2]. Their usage in the biological and medical domains is constrained due to the use of hazardous chemicals, the difficulty of the synthesis process, the high pricing, and the creation of dangerous by-products [3].

In a green way to generate nanoparticles, plant extracts are used to generate nanoparticles that are easy, fast, and do not contain toxic or high-energy substances. Additionally, diverse proteins found in microbes and plant extracts serve as capping agents, allowing the creation of nanoparticles to be scaled up [4]. The use of plant extracts has some perks over the utilization of microorganisms among the various organisms that are used to produce nanoparticles, such as the absence of the need for culture media or other challenges associated with the use of microorganisms for nanoparticle production, such as the need for aseptic conditions [5]. The utilization of plants is now one of the most dependable processes for synthesizing nanoparticles due to the usage of biomaterials, green, and ease of synthesis [6]. Plant extracts include coating and reducing substances such as polysaccharides, amino acids, flavonoids, terpenes, enzymes, and proteins. These substances may generate nanoparticles with remarkable stability and a variety of sizes and forms by reducing metal ions [7].

Recent years have seen a plethora of basic and medicinal uses for magnetic nanoparticles (Fe_3O_4, γ-Fe_2O_3, α-Fe_2O_3, and FeO). Hematite (α-Fe_2O_3), a more stable form of iron oxide than other polymorphs, has a range of useful technological uses due to its low cost, superior chemical stability, anti-corrosive, tuneable optical, and magnetic characteristics [8]. Iron oxide nanoparticles have gained much attention

* **Corresponding author: Abdullah R. Alzahrani,** Department of Pharmacology and Toxicology, Faculty of Medicine, Umm Al-Qura University, Makkah 77207, Saudi Arabia, e-mail: aralzahrani@uqu.edu.sa

because of their distinct physiochemical characteristics. Using green chemistry, plants can generate iron oxide nanoparticles, which is a revolutionary way that gets beyond the drawbacks of existing traditional approaches. In this green route of the fabrication process, the biomolecules of plants serve as capping and reducing agents [9]. These therapeutic efficacies are due to the bioactive components that are affixed to the NPs' surface. These characteristics are also connected to the biological uses of NPs. In the combat against oxidative stress, the weakly radical scavenging action is efficient [10]. Additionally, ROS may be transported into bacteria via iron-oxide (Fe_2O_3) nanoparticles, which disrupts the functionality of the cell membrane and causes the leaking of cellular components, which may induce bacterial cell death [11].

Traditional medicine places a special emphasis on therapeutic herbs from the genus Berberis. Several studies have reported that among distinct Berberis species, the *Berberis vulgaris* plant has pharmaceutical, antioxidant, and nutritional properties [12]. The different organs of this plant contain several alkaloids, the most significant of which is berberine. This alkaloid can have a variety of effects, including anti-inflammatory, hypoglycemic, antioxidant, and hypotensive properties [13]. The culinary and pharmaceutical sectors employ various *B. vulgaris* organs, while the ornamental species are used to beautify various locations. Traditional medicine recommends using *B. vulgaris* to treat liver illness, hyperlipidemia, hyperglycemia, depression, and bleeding [14]. According to the findings, *B. vulgaris* includes a substantial number of phytochemical substances, including more than ten phenolic compounds, vitamin K, ascorbic acid, a variety of triterpenoids, and more than thirty alkaloids [15]. Consequently, *B. vulgaris* may have benefits that are antioxidant, analgesic, hepatoprotective, anti-inflammatory, antibacterial, anti-cancer, and anti-inflammatory [12].

Recent research has focused heavily on the surface modification of nanoparticles by polymers to diminish aggregation, regulate their physicochemical characteristics, and regulate their links with biological systems [16]. The polymer can increase the nanoparticles' stability in the cellular environment and improve their biocompatibility with healthy, normal live cells and organs [17]. As a surfactant polyol, Pluronic F127 exhibits a low toxicity that allows it to be used to control drug release while also facilitating the solubilization of water-insoluble materials in physiological media, as well as acting as an absorption promoter that improves drug permeability across ocular epithelia [18]. A commercially available FDA-approved triblock copolymer called Pluronic F-127 is among these polymers. It is injectable, nontoxic, biocompatible, and thermo-reversible [19]. It can exhibit amphiphilic properties in an aqueous environment. Pluronic F-127 is ideally suited for gene therapy, controlled release, drug administration, and tissue engineering because of its unique thermo-reversible micellization property near body temperature [20].

The results showed that both synthesized FeO-NPs displayed 100% antimicrobial photodynamic therapy activity after light-emitting diode irradiation. The water extract of FeO-NPs and methanol extract of FeO-NPs also showed significant biofilm inhibition [21]. The study synthesized hematite nanoparticles using Artemisia plant extract, achieving a saturated magnetization of 0.96 $emu \cdot g^{-1}$ and a low remnant magnetization of 0.06 $emu \cdot g^{-1}$, indicating potential biomedical applications [22]. The study reveals that green iron nanoparticles with high adsorption capacity are promising for industrial applications. Clove-prepared iron nanoparticles showed more effective bactericidal activity against pathogens than g-Coffee-prepared ones, with Clove-prepared iron oxide inhibiting *Staphylococcus aureus* and *Escherichia coli* at different depths [23]. The study showcases the green synthesis of Fe_2O_3 nanoparticles from *Bauhinia tomentosa* leaf extract, demonstrating their effectiveness in lipase immobilization and 1,3-diolein synthesis [24].

In this work, Pluronic F-127-coated Fe_2O_3 NPs were prepared using a novel, environmentally friendly method, and their characterization studies including ultraviolet-visible (UV-Vis), Fourier transform infrared (FTIR), dynamic light scattering (DLS), X-ray diffraction (XRD), photoluminescence (PL), scanning electron microscopy (SEM) with EDAX, and transmission electron microscopic (TEM) analysis were performed. In addition, the antibacterial biological cytotoxicity and antioxidant activity of fabricated Pluronic F-127-coated Fe_2O_3 NPs were assessed for the first time to our knowledge. Fe_2O_3 NP's stability and biocompatibility have been markedly enhanced by the modification method while also maintaining their preferred crystalline form.

2 Materials and methodology

2.1 Preparation of *B. vulgaris* extract

A freshly harvested *B. vulgaris* plant, authenticated by the Botanical Survey of India (11.6653454; 78.280684), weighed 10 g and was soaked in 100 mL of demineralized water for 20 min at 80°C. Using Whatman No. 1 filter paper, the resulting extraction was purified. The filtrate was then stored in a 250 mL Erlenmeyer flask and kept at 37°C for further processing.

2.2 Preparation of Fe_2O_3 NPs

To synthesize Fe_2O_3 NPs, 0.5 g of Pluronic F-127 and 0.1 M of ferrous nitrate hexahydrate $Fe(NO_3)_2{\cdot}6H_2O$ were mixed in 100 mL of prepared *Berberis vulgaris* extract. This resulted in a red-colored homogenous reaction mixture. This mixture was continuously agitated for 5 h at a temperature of 80°C. At 120°C for 1 h, the resulting crimson precipitate was dried. For further research, the obtained Fe_2O_3 NPs in powder state were annealed at a temperature of 800°C for 5 h.

2.3 UV-Vis spectroscopic analysis of PF127Fe_2O_3NPs

UV-Vis spectroscopy was used to identify the surface plasmon resonance peak in the Fe_2O_3 nanoparticle. Analyzed nanoparticle samples were carried out at wavelengths ranging from 200 to 1,100 nm. To calculate the average absorbance of the Fe_2O_3 nanoparticle, the experiment was carried out three times.

2.4 Analysis of PF127Fe_2O_3NPs by DLS

The Fe_2O_3 nanoparticle was examined using DLS. The nanoparticles were first homogenized with Milli-Q water, and then the mixture was subjected to 30 s of sonication. Nanoparticles are diluted 1:10 with Milli-Q water before undergoing a zeta potential test.

2.5 Analysis of PF127Fe_2O_3NPs with field emission-scanning electron microscopy (FESEM) and EDAX

FESEM coupled with EDAX was used to examine the composition, size, and surface properties of the fabricated Fe_2O_3 nanoparticle.

2.6 TEM analysis of PF127Fe_2O_3NPs

The TEM (Tecnai F20 model) apparatus was used to analyze the morphologies of the PF127Fe_2O_3NPs at a 200 kV accelerating voltage.

2.7 XRD analysis of PF127Fe_2O_3NPs

An XRD was used to analyze the PF127Fe_2O_3NPs. When the monochromatic wavelength of 1.54 Å was employed, the diffraction patterns for the PF127Fe_2O_3NPs were recorded in the 20°–80° range.

2.8 FTIR spectroscopic analysis of PF127Fe_2O_3NPs

Investigation of the different functional groups present in Fe_2O_3 NPs was done using FTIR analysis. Potassium bromide pellets and Fe_2O_3 NPs were mixed in a 1:100 ratio before being scanned at a resolution of 4 cm, each scan between 500 and 4,000 cm^{-1}. The program was used to perform and assess 50 scans in total.

2.9 PL analysis of PF127Fe_2O_3NPs

The electronic structure and characteristics of the PF127 Fe_2O_3NPs were assessed using photoluminescence spectroscopy (Cary Eclipse spectrometer).

2.10 Determination of antibacterial potential of PF127 Fe_2O_3NPs

The antibacterial activity of the PF127Fe_2O_3NPs was examined by the well diffusion technique and tested against *Bacillus subtilis*, *Klebsiella pneumoniae*, *S. aureus*, *Streptococcus pneumoniae*, *E. coli*, and *Shigella dysenteriae* following molten nutritional agar. Micropipettes were used to transfer test samples at concentrations of 1, 1.5, and 2 $mg{\cdot}mL^{-1}$ onto the bacteria-seeded well plates. Following that, the plates were incubated at 37°C for a duration of 24 h. The inhibition zone's dimensions were taken. The positive control against *B. subtilis*, *K. pneumoniae*, *S. aureus*, *S. pneumoniae*, *E. coli*, and *S. dysenteriae* was amoxicillin (Hi-Media) [21].

2.11 Estimation of *in vitro* antioxidant activity of PF127 Fe_2O_3NPs

The antioxidant capability of the Pluronic F-127 encapsulated Fe_2O_3 nanoparticles was studied by 1,1-diphenyl-2-picrylhydrazyl (DPPH) radical scavenging activity. Each

test is carried out three times. Several concentrations of Fe_2O_3 NP solution (2, 4, 8, 16, 32, and 64 μg·mL^{-1}) were mixed with an equivalent volume of 0.1 mM DPPH solution. The reaction mixture's absorbance at 517 nm was measured after it had been incubated for a duration of 30 min at 37°C and in the dark. The application of ascorbic acid as the benchmark and ethanol (blank) as the positive control. It is proof of antioxidants' ability to scavenge free radicals that the absorbance of the DPPH mixed reaction mixture reduced when the antioxidant was introduced. The percentage of free radicals that were suppressed or scavenged was calculated using the following formula:

$$\%\text{of scavenging activity} = \frac{[\text{Value of optical density} \in \text{control sample} - \text{Values} \in \text{the experimental sample}]}{\text{Value of optical density} \in \text{control sample}} \times 100 \quad (1)$$

2.12 Cell viability assay

The study used Vero (normal), MDA MB-231, and MCF-7 breast cancer cell lines to assess PF127Fe_2O_3NPs cytotoxicity based on Sarathbabu et al. [22]. Cells were seeded onto 96-well tissue culture plates and incubated with Fe_2O_3 NPs for 24, 48, and 72 h at room temperature and 5% CO_2. After incubation, 3-[4,5-dimethylthiazol-2-yl]-2,5 diphenyl tetrazolium bromide (MTT) was added for 2–4 h until purple crystallites appeared. Cells were drained and cleaned with 1× PBS. Viability percentage and IC_{50} value were calculated using GraphPad Prism 6.0 software.

$$\text{Cell viability\%} = \frac{\text{Optical density of sample}}{\text{Optical density of control}} \times 100 \quad (2)$$

2.13 Statistical analysis

Each study was conducted in triplicate, and the results were statistically analyzed using One-way ANOVA and a *post hoc* Tukey post-test. The results were presented as mean ± SD, with $P < 0.05$ considered statistically significant.

3 Results and discussion

3.1 UV-Vis spectra of PF127Fe_2O_3NPs

From the highest occupied molecular orbital in the valence band (VB) to the lowest unoccupied molecular orbital in the conduction band (CB), electrons are excited by the absorption of electromagnetic waves. By absorbing wavelengths between bonding and anti-bonding orbitals, the substance's band gap energy can be determined. The three probable electronic transitions between 200 and 1,000 nm are n → π, n → σ*, and π → π* [23]. With a UV-Vis spectrophotometer operating at room temperature, the optical absorbance of Fe_2O_3 nanoparticles was examined; the corresponding spectrum is shown in Figure 1. Using UV-Vis spectroscopy, it is possible to determine if precursor reduction has been placed. The presence of Fe_2O_3 NPs is indicated by a high absorption peak at 395 nm [24]. The absorption bands observed at 395 nm are caused by the ligand-to-metal charge-transfer transitions (direct transitions), with coupled effects from the Fe^{3+} ligand field transitions [25].

3.2 FTIR spectra of PF127Fe_2O_3NPs

The *B. vulgaris* extract used to make Fe_2O_3 NPs was subjected to FTIR examinations to look for any potential modifications in functional group bonds that could have occurred through the reduction process. Figure 2 illustrates the FTIR spectrum for PF127Fe_2O_3NPs mediated by *B. vulgaris* extract, which showed multiple distinct bands at 463, 555, 1,050, 1,113, 1,422, 1,647, 2,854, 2,924, and 3,419 cm^{-1}, respectively. *B. vulgaris* extract has a shifted absorption band at 555 cm^{-1}, and the band at 463 cm^{-1} matches the Fe–O stretch of Fe_2O_3, demonstrating the synthesis of Fe_2O_3 NPs. The intensity of the detected absorption bands exceeded those of the extract, demonstrating the extract's reducing function in forming

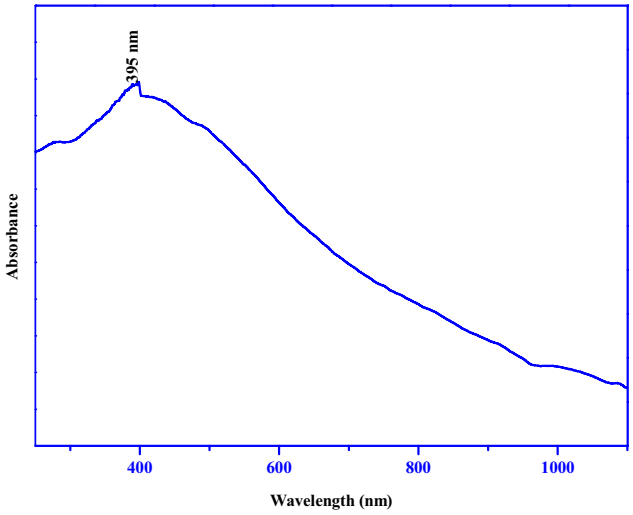

Figure 1: UV-Vis spectrophotometer analysis of synthesized Pluronic F-127 coated Fe_2O_3 NPs. Fe_2O_3 nanoparticles coated with Pluronic F-127 and analyzed with a UV-Vis spectrophotometer.

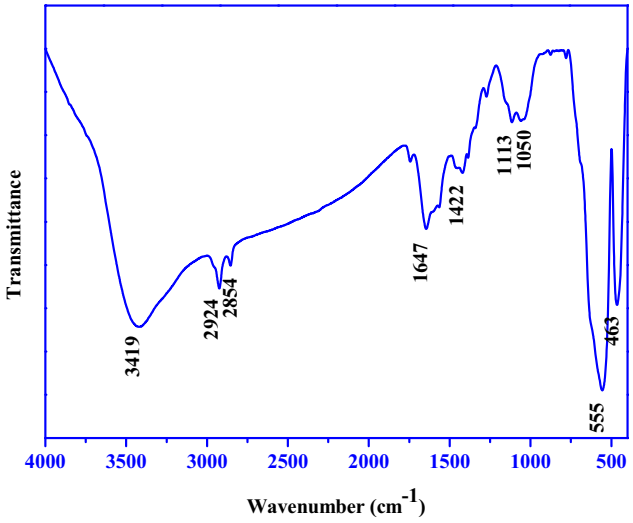

Figure 2: FTIR analysis of Pluronic F-127 coated Fe_2O_3 NPs derived from infrared analysis. Based on infrared analysis, FTIR transmission vs wavenumber of pluronic F-127 coated Fe_2O_3 nanoparticles is depicted in the chart.

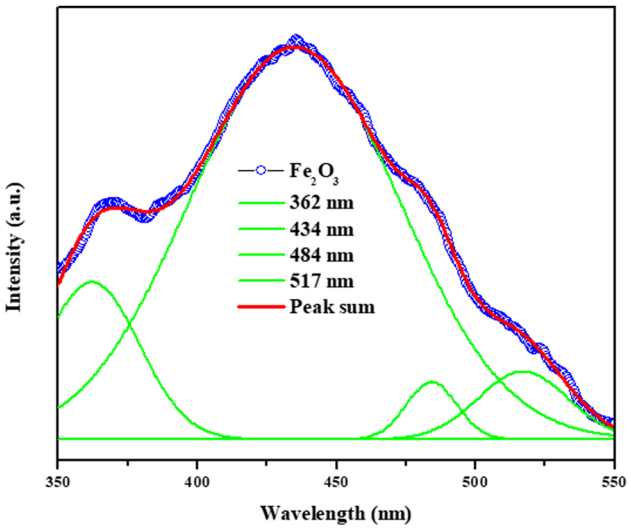

Figure 3: PL spectroscopy spectrum of Pluronic F-127 coated Fe_2O_3 NPs. Fe_2O_3 nanoparticles coated with Pluronic F-127 and their PL spectrum.

Fe_2O_3 NPs. The peak at 1,113 cm^{-1} represents the stretching vibration of the C–O–C present in the polyphenolic chemicals that are found in the plant extract. The in-plane bending vibrations of O–H in phenols correspond to the band obtained at 1,422 cm^{-1}. The polyphenol chemicals found in the plant extract and the amino acids that stabilized and served as a capping agent are shown by the absorption band at 1,647 cm^{-1}, which is related to the C═O bond stretching. To reduce iron ions and iron oxide nanoparticles, polyphenol compounds and phenyl groups are crucial [26,27]. C–H stretching peaks present in Pluronic F-127 were seen at 2,924 and 2,854 cm^{-1}, respectively. The band with the maximum intensity that is ascribed to the O–H groups is an indication that the surface of the manufactured Fe_2O_3 NPs has been coated with water-soluble polyphenol compounds. With an enhanced absorption band, the ferric chloride reduction is shown by the band at 3,419 cm^1, which corresponds to the O–H bond stretching and identifies the aqueous phase [28,29].

3.3 PL spectra of PF127Fe_2O_3NPs

A key method for assessing the optical characteristics of electronic materials is PL analysis. Fabricated Fe_2O_3 NPs' PL spectra at room temperature are depicted in Figure 3 and stimulated at a wavelength of 325 nm (Figure 3). The PF127Fe_2O_3NPs' PL emission spectra showed values at 362, 434, 484, and 512 nm, respectively. The VB and CB are excited, resulting in 362 nm UV emission. Excitons and holes flow freely in CB and VB, generating excitons. Blue emission at 434 and 484 nm is caused by electron and hole recombination, while green emission at 512 nm is caused by ionized oxygen vacancies and structural flaws in Fe_2O_3 NPs [30–32].

3.4 Morphological analysis of PF127Fe_2O_3NPs

Nanostructured hematite particles' shape, size, and crystallinity were confirmed using TEM imaging and Selected area (electron) diffraction [SAED] pattern analysis, revealing spherical structure (Figure 4(a–d)). To further demonstrate the crystallinity of the distinct little bright and pointed dots that make up the ring, which is coated with Pluronic F-127. The SAED pattern confirmed the rhombohedral crystalline phase of the produced Fe_2O_3 NPs (Figure 4e). This agrees with XRD data and TEM micrographs that demonstrate that all the particles are nanoscale in size.

3.5 FESEM analysis and EDAX spectra of PF127Fe_2O_3NPs

The PF127Fe_2O_3NPs were synthesized using *Berberis vulgaris* extract at room temperature utilizing a green approach. The PF127Fe_2O_3NPs SEM study monitored Fe_2O_3 NPs' shape, and the particle size ranged from 35 to 55 nm. According to Figure 5(a and b), the particles were agglomerated and spherical. The presence of biological substances on the surface of

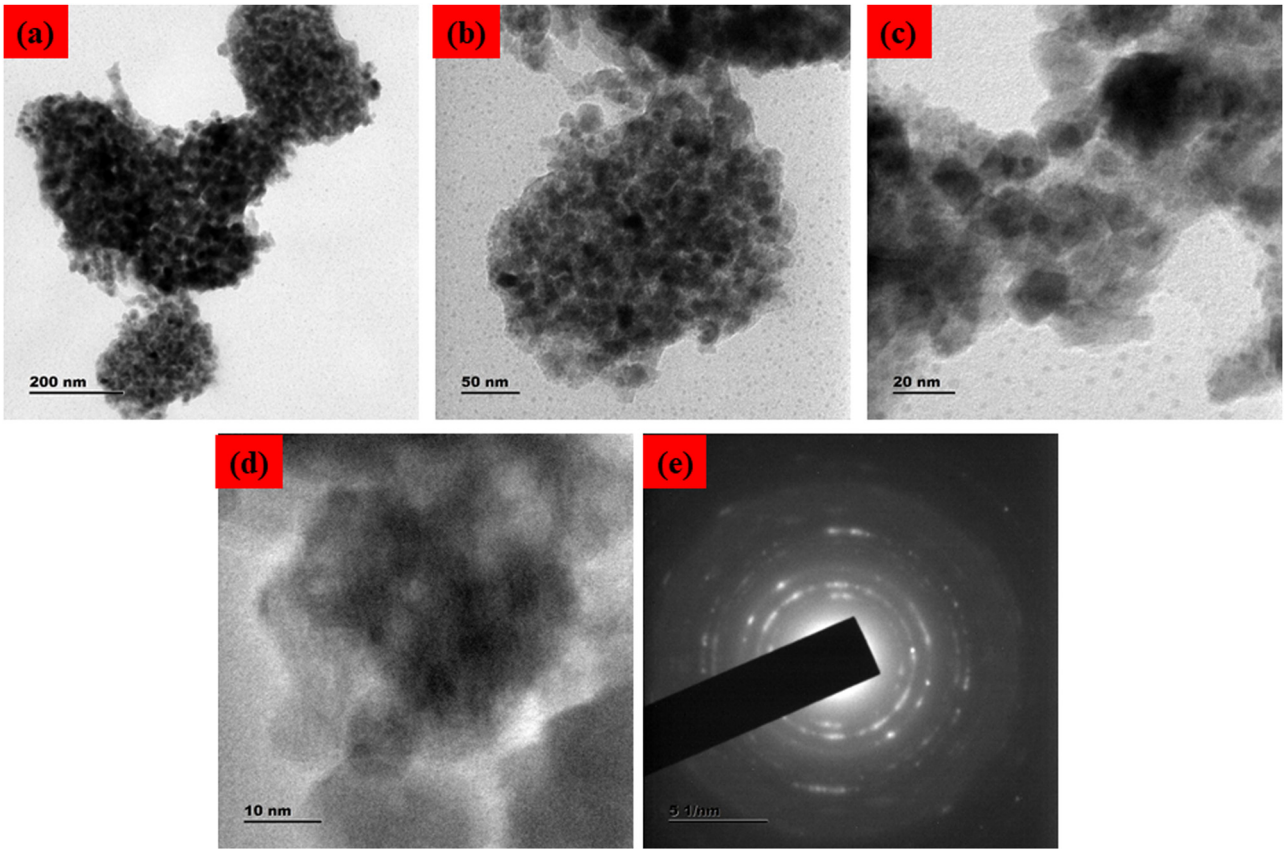

Figure 4: TEM micrographics of the Pluronic F-127 coated Fe_2O_3 NPs: lower (a, b) and higher (c, d) magnification TEM image and SAED pattern (d). PF127Fe_2O_3NPs TEM study monitored Fe_2O_3 NPs' shape, with particle sizes ranging from 30 to 50 nm.

the particles may be the cause of the agglomeration. The particles seem to aggregate because bioactive chemicals had OH bonding, which makes this possible (Figure 5c) [33–35].

3.6 X-ray diffraction patterns of PF127Fe_2O_3NPs

Figure 6 displays the XRD spectrum of the green route fabricated PF127Fe_2O_3NPs. The generation of α-Fe_2O_3 NPs was indicated by well-defined peak locations in the XRD spectra with 2θ values of (012), (104), (110), (113), (024), (116), and (018) corresponding to the 25.160°, 35.120°, 36.630°, 40.640°, 49.970°, 57.080°, and 59.420°. The crystalline nature of the Fe_2O_3 NPs produced by the reduction technique utilizing *B. vulgaris* extract was unquestionably demonstrated by the strong and crisp peaks. The findings nearly exactly match those of other researchers who studied iron oxide nanoparticles [26,36], supporting the creation of a crystalline rhombohedral structure. According to the Debye–Scherrer equation [26], the average crystallite size of synthetic PF127Fe_2O_3NPs was 32.54 nm. The computed lattice parameters are a = 0.506 nm and c = 1.388 nm. The absence of additional diffraction peaks suggests that the PF127Fe_2O_3NPs produced by green synthesis were very pure and had high crystallinity.

3.7 DLS spectra of PF127Fe_2O_3NPs

Figure 6 displays the particle size distributions for PF127Fe_2O_3NPs. The average diameter of the particles after 800°C annealing is 174.90 nm. The build-up of primary particles results in an expansion in the mean particle size.

3.8 Antibacterial effect of PF127Fe_2O_3NPs

The antibacterial activity and zone of inhibition of fabricated PF127Fe_2O_3NPs are depicted in Figure 7. PF127Fe_2O_3NPs exhibit antibacterial activity against bacterial strains including *B. subtilis*, *S. pneumonia*, *E. coli*, *S. aureus*, *K. pneumonia*, and *S. dysenteriae* bacterial strains. Amoxicillin samples and

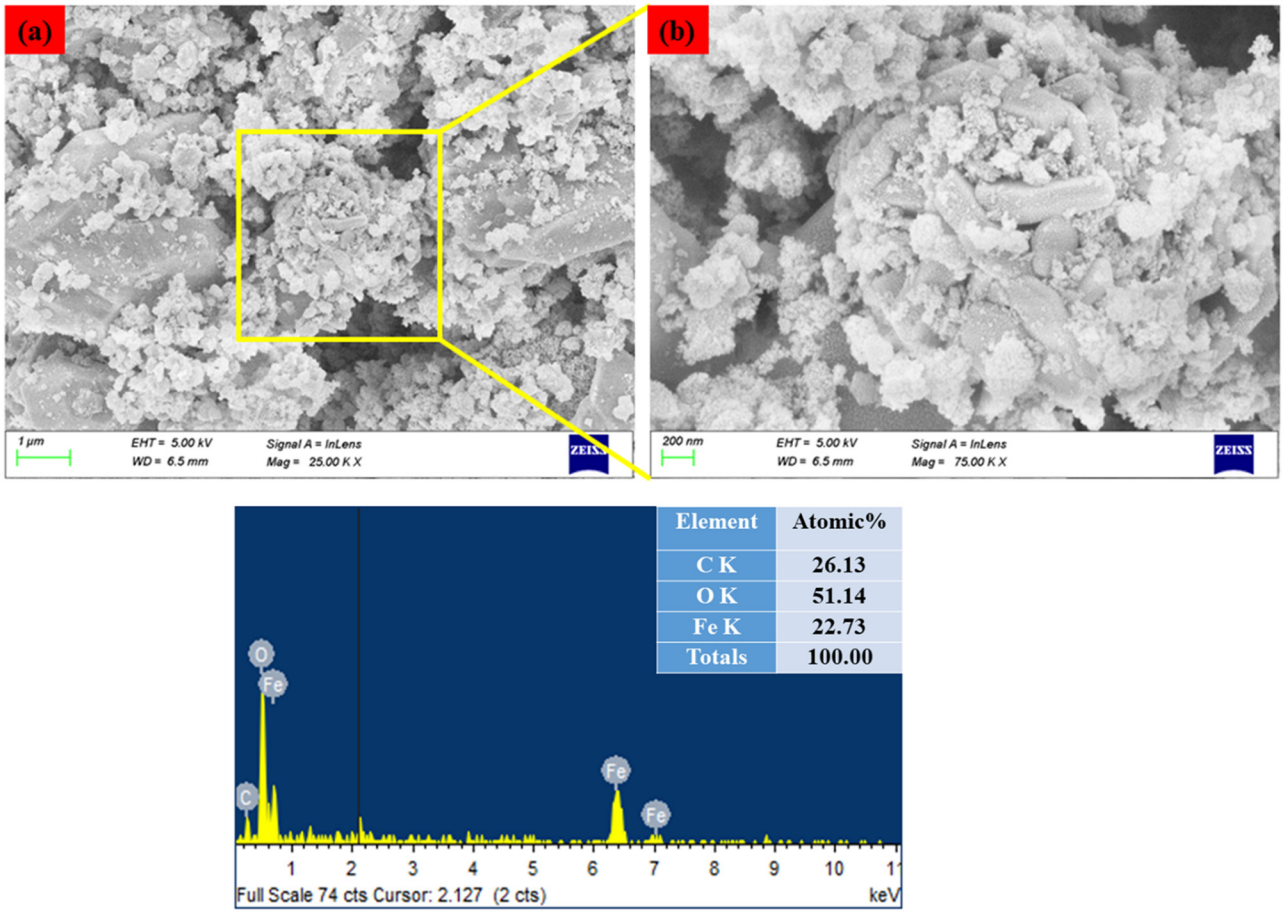

Figure 5: FESEM image of Pluronic F-127 coated Fe_2O_3 NPs. Lower (a) and higher (b) magnification. Elements, weight %, and atomic % of the composition obtained by EDX (c).

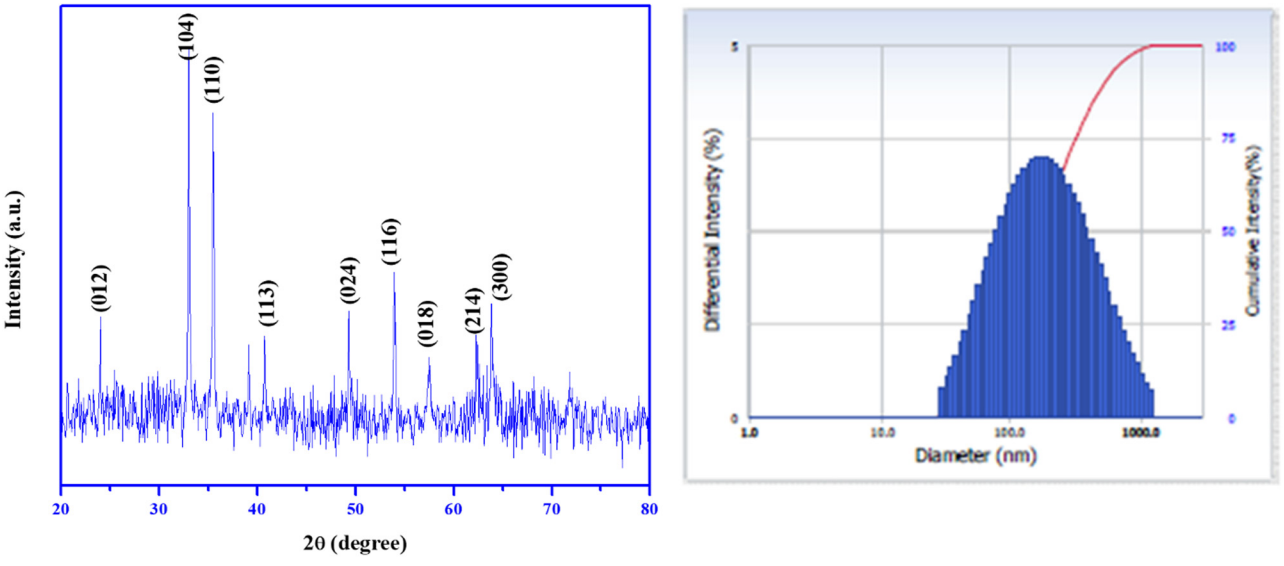

Figure 6: X-ray diffraction analysis (XRD) pattern and DLS Spectrum of Pluronic F-127 coated Fe_2O_3 NPs. Fe_2O_3 NPs coated with Pluronic F-127 and their XRD patterns and DLS spectra.

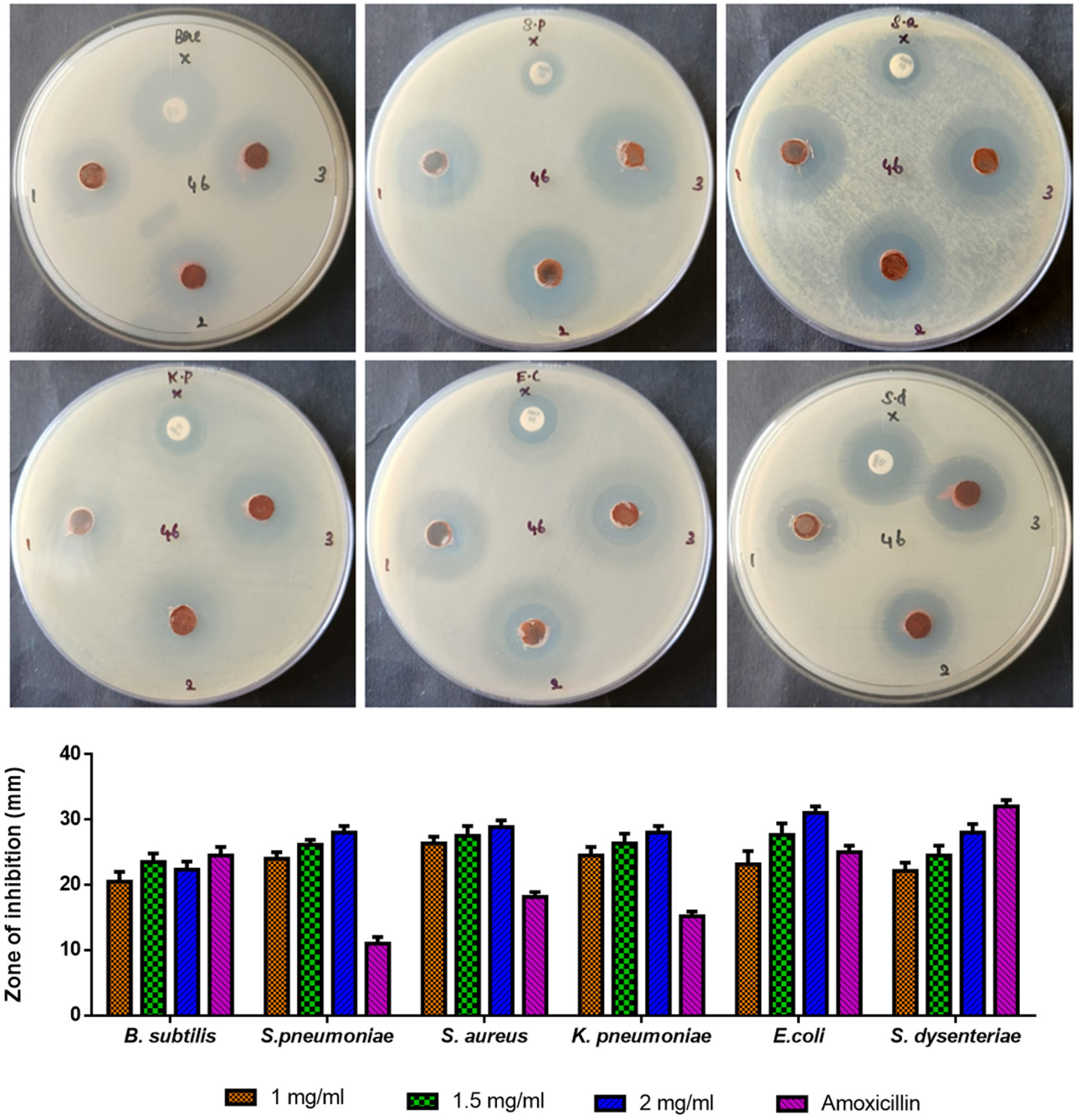

Figure 7: Antibacterial activity of Pluronic F-127 coated Fe_2O_3 NPs. NPs inhibit the growth of bacteria and a zone of inhibition was shown in agar well plates. Graphical representation of antibacterial activity was determined for Pluronic F-127 coated Fe_2O_3 NPs by measuring the zone of inhibition (mm).

fabricated PF127Fe_2O_3NPs both demonstrate antibacterial activity. PF127Fe_2O_3NPs have a stronger antibacterial effect as compared to amoxicillin. Additionally, the antimicrobial activity increased as NP concentration was raised. The fact that Fe_2O_3 NPs are highly stable in the ambient environment, indicating that metal ion release plays a lesser role in antibacterial activity, is one of the proposed pathways by which Fe_2O_3 NPs are effective against bacteria [37]. Contrarily, exposure to UV light causes the defect sites of Fe_2O_3 to create visible light electron–hole pairs or to produce reactive oxygen species. The electron–hole pairs that are created can help ROS like superoxide radical anions (O_2^-) and hydroxyl radicals (OH^-) generate. The OH^- and O_2^- free radicals generated can destroy the membrane, thereby

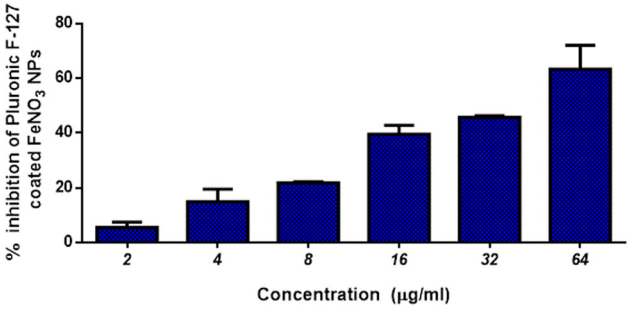

Figure 8: Antioxidant activity and percentage of inhibition DPPH free radical by synthesized Pluronic F-127 coated Fe_2O_3 NPs. An illustration of the antioxidant activity (superoxide radical scavenging activity) of Pluronic F-127 coated Fe_2O_3 NPs is provided. The values are presented as means and standard deviations (n = 3).

eradicating the microorganisms [38]. Furthermore, cellular function disruption and membrane disarray are caused by important interactions such as dipole–dipole, hydrophobic, electrostatic, hydrogen bond, and van der Wall's contacts [34].

3.9 Antioxidant activity and percentage of inhibition of DPPH free radical by synthesized PF127Fe_2O_3NPs

Potential free radical scavenging capacity against DPPH free radicals is shown by Fe_2O_3 nanoparticles in Figure 8. The radical DPPH is transformed into the colorless stable diamagnetic compound by the NPs by transferring electrons or hydrogen to it. In previous studies, flavonoids and phenolics were noted to be present in *B. vulgaris* plants [39], which have been used to form nanoparticles encapsulating Fe_2O_3 using Pluronic F-127. The phenolic and flavonoid-rich plant extract serves as a reducing agent for the fabrication of nanoparticles [40]. A range of biological applications are available from phenolic compounds in edible and medicinal plants, including epigallocatechin gallate, catechins, ferulic acid, flavonoids, proanthocyanidins, and tannins [41]. The redox characteristics of phenolic compounds, which can be useful in the captivation and nullification of free radicals, dissolving peroxides, or quenching singlet and triplet oxygen, are primarily responsible for their antioxidant action [42]. In this study, the DPPH scavenging activity ranges from 5% to 70% for the five distinct concentrations of iron oxide NPs, which are 20, 30, 40, 50, 60, and 70 $\mu g \cdot mL^{-1}$. The scavenging mechanism elevates with the increasing concentration of Fe_2O_3 NPs. The trend observed in the scavenging activity is 64 > 32 > 16 > 8 > 4 > 2 $\mu g \cdot mL^{-1}$ of Fe_2O_3 NPs. When the DPPH radical interacts with the surface of Fe_2O_3 NPs, an electron is transferred from the oxygen species to the nitrogen atom of the DPPH, which scavenges the radical. So, Fe_2O_3 NPs exhibit effective antioxidant activity and can be used for therapeutic purposes.

3.10 Effect of PF127Fe_2O_3 NPs on cell viability

MTT assay assessed iron oxide nanoparticles' cytotoxic activity against MCF7, MDA-MB-231, and Vero cell lines. Figure 9 depicts the cytotoxic effect of fabricated Fe_2O_3 NPs (2–64 $\mu g \cdot mL^{-1}$) for 24, 48, and 72 h. The MTT test, which relies on actively developing cells to generate blue, water-insoluble formazan crystals, has been frequently used to gauge the rate of cell proliferation. The concentration of the Fe_2O_3 NPs had an impact on the cell viability, which reduced as the concentration of Fe_2O_3 NPs increased. The IC_{50} value for the MCF7 (breast) cell line was calculated to be 21.9, 44.18, and 51.58 $\mu g \cdot mL^{-1}$ for 24, 48, and 72 h respectively. The IC_{50} value for the MDA-MB-231 (breast) cell line was calculated to be 27.17, 45.64, and 75.96 $\mu g \cdot mL^{-1}$ for 24, 48, and 72 h, respectively. The small impact of all samples on normal cell lines supports the unique impact of fabricated Fe_2O_3 NPs on cancer cells. It has been noted that mitochondria, which are redox-active organelles, are attacked by nanoparticles of various sizes and chemical compositions. In cells exposed to nanoparticles, mitochondria are a key location for ROS production. In the fabrication of nanoparticles, Flavonoids and Phenolics are found in *B. vulgaris* leaf extract to serve as a reducing agent and capping agent, respectively. PF127$Fe_2O_3NP_s$ have a lower toxicity risk. As a result of the controlled release of encapsulated Fe_2O_3 nanoparticles, there is a reduced risk of quick increases in ROS in breast cancer cells, which leads to a gradual increase in their cytotoxicity. Nanoparticles may cause oxidative stress by altering ROS and influencing antioxidant defenses [43,44]. Hydrogen peroxide ($H_2O_2^-$), superoxide radical (O_2^-), and hydroxyl radical (OH^*) are the most common ROS, and they damage biological components, including DNA, leading to apoptotic cell death [45]. This makes it evident that Fe_2O_3 NPs react in a similar way in MCF7 (breast) and MDA-MB-231 (breast) to induce apoptosis. Other than iron nanoparticles, the previous study explores the green synthesis of silver nanoparticles using *Carissa spinarum* leaf extract, revealing its potential as a rapid, cheap, and effective mosquitocides bio-resource [46]. The previous study presents a hybrid nanosystem for cancer-targeted fluorescence imaging and drug delivery, enhancing antibiofilm and antioxidant properties, with potential applications in various industries [47].

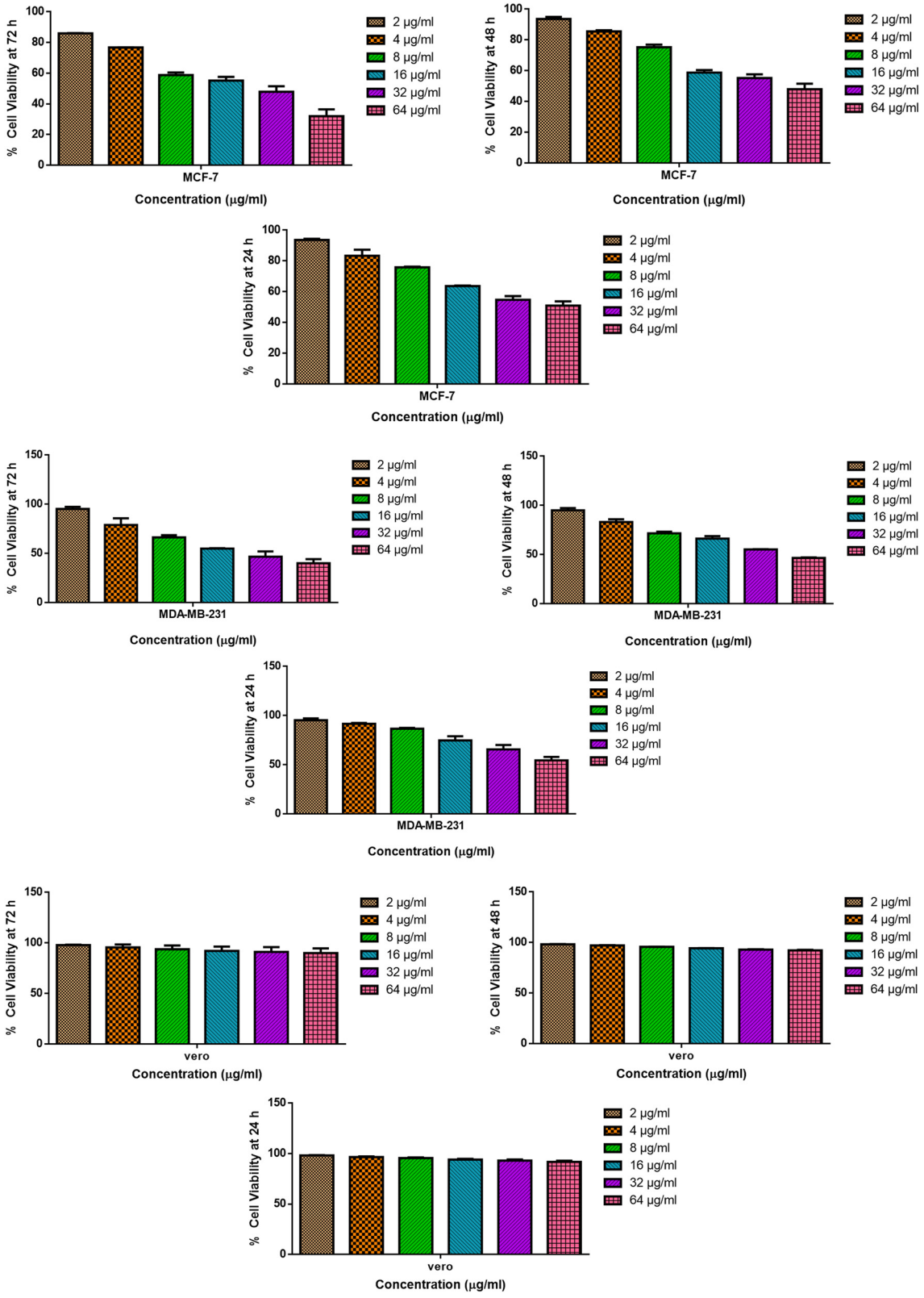

Figure 9: Pluronic F-127 coated Fe_2O_3 NPs cause cytotoxicity in MCF7 (breast), MDA-MB-231(breast), and Vero cells. MCF7 (breast), MDA-MB-231(breast), and Vero cell lines were treated with different concentrations (2–64 µg·mL^{-1}) of Pluronic F-127 coated $FeNO_3$ NPs for 24, 48 and 72 h. The cells were subjected to MTT assay and the values were depicted as ±SD of three individual experiments.

The study explored a novel approach to cancer research by investigating the potential anticancer properties of nanoparticles derived from *B. vulgaris* extract and encapsulated in Pluronic F-127. The study explores the anticancer potential of Pluronic F-127 encapsulated Fe_2O_3 nanoparticles derived from *B. vulgaris* extract. The innovative formulation technique combines a natural extract with a biocompatible polymer, potentially enhancing the nanoparticles' properties and applications. The nanoparticles effectively inhibit cancer cell proliferation, indicating their potential as an anticancer drug. They also exhibit antimicrobial properties against gram-negative and gram-positive bacteria. The study also highlights a dose-dependent effect on breast cancer cells (MCF7 and MDA-MB-231), highlighting the potential dosage for achieving desired anticancer effects. The nanoparticles also show enhanced antioxidant activity, suggesting their dual potential as an antioxidant and anticancer agent.

4 Conclusion

In the current research, we have fabricated an effective nanoparticle utilizing Pluronic F-127 as an effective delivery agent and *B. vulgaris* leaf extract as a reducing and capping agent. The characterization studies of the nanoparticles revealed the formation of a complete nanoparticle and the presence of all the components in the nanoparticle. We have also analyzed the effect of fabricated nanocomposite on microbes, cell viability of the MCF7 (breast), MDA-MB-231 (breast), Vero cell lines, and antioxidant activity. These results confirmed the potency of pluronic F-127-encapsulated Fe_2O_3 nanoparticles as an anticancer drug and antioxidant. Furthermore, considerable research is required in the long term to determine the precise therapeutic mechanisms of the Pluronic F-127 encapsulated Fe_2O_3 nanoparticle.

Acknowledgments: The author acknowledges the support given by the institution (Department of Pharmacology and Toxicology, Faculty of Medicine, Umm Al-Qura University, Makkah 77207, Saudi Arabia) for conducting this study.

Funding information: Author states no funding involved.

Author contributions: The author contributed to the work.

Conflict of interest: Author states no conflict of interest.

Data availability statement: The datasets generated during and/or analyzed during the current study are available from the corresponding author on reasonable request.

References

[1] Jeevanandam J, Barhoum A, Chan YS, Dufresne A, Danquah MK. Review on nanoparticles and nanostructured materials: history, sources, toxicity, and regulations. Beilstein J Nanotechnol. 2018 Apr;9:1050–74. doi: 10.3762/bjnano.9.98, PMID: 29719757; PMCID: PMC5905289.

[2] Yetisgin AA, Cetinel S, Zuvin M, Kosar A, Kutlu O. Therapeutic nanoparticles and their targeted delivery applications. Molecules. 2020 May;25(9):2193. doi: 10.3390/molecules25092193. PMID: 32397080; PMCID: PMC7248934.

[3] Gupta RB. Fundamentals of drug nanoparticles. In: Nanoparticle Technology for Drug Delivery. Florida, United States: CRC Press; 2006. p. 25–44.

[4] Parveen K, Banse V, Ledwani L. Green synthesis of nanoparticles: Their advantages and disadvantages. AIP Conf Proc. 2016;1724:020048. doi: 10.1063/1.4945168.

[5] Nikbakht M, Yahyaei B, Pourali P. Green synthesis, characterization and antibacterial activity of silver nanoparticles using fruit aqueous and methanolic extracts of Berberis vulgaris and Ziziphus vulgaris. J Pure Appl Microbiol. 2015;9(1):349–55.

[6] Singh J, Dutta T, Kim KH, Rawat M, Samddar P, Kumar P. 'Green' synthesis of metals and their oxide nanoparticles: applications for environmental remediation. J Nanobiotechnol. 2018;16:84. doi: 10.1186/s12951-018-0408-4.

[7] Afshar AS, Nematpour FS. Evaluation of the cytotoxic activity of biosynthesized silver nanoparticles using Berberis vulgaris leaf extract. Jentashapir J Cell Mol Biol. 2021;12(1):e112437.

[8] Pallela PNVK, Ummey S, Ruddaraju LK, Gadi S, Cherukuri CS, Barla S, et al. Antibacterial efficacy of green synthesized α- Fe_2O_3 nanoparticles using Sida cordifolia plant extract. Heliyon. 2019;5(11):e02765.

[9] Jagathesan G, Rajiv P. Biosynthesis and characterization of iron oxide nanoparticles using Eichhornia crassipes leaf extract and assessing their antibacterial activity. Biocatalysis Agric Biotechnol. 2018;13:90–4.

[10] Naz S, Islam M, Tabassum S, Fernandes NF, de Blanco EJC, Zia M. Green synthesis of hematite (α- Fe_2O_3) nanoparticles using Rhus punjabensis extract and their biomedical prospect in pathogenic diseases and cancer. J Mol Structure. 2019;1185:1–7.

[11] Bashir M, Ali S, Farrukh MA. Green synthesis of Fe_2O_3 nanoparticles from orange peel extract and a study of its antibacterial activity. J Korean Phys Soc. 2020;76(9):848–54.

[12] Rahimi-Madiseh M, Lorigoini Z, Zamani-Gharaghoshi H, Rafieian-Kopaei M. Berberis vulgaris: specifications and traditional uses. Iran J Basic Med Sci. 2017;20(5):569.

[13] Neag MA, Mocan A, Echeverría J, Pop RM, Bocsan CI, Crişan G, et al. Berberine: botanical occurrence, traditional uses, extraction methods, and relevance in cardiovascular, metabolic, hepatic, and renal disorders. Front Pharmacol. 2018 Aug;9:557. doi: 10.3389/fphar.2018.00557. PMID: 30186157; PMCID: PMC6111450.

[14] El-Zahar KM, Al-Jamaan ME, Al-Mutairi FR, Al-Hudiab AM, Al-Einzi MS, Mohamed AA. Antioxidant, antibacterial, and anti-fungal activities of the ethanolic extract obtained from berberis vulgaris roots and leaves. Molecules. 2022 Sep;27(18):6114. doi: 10.3390/molecules27186114, PMID: 36144846; PMCID: PMC9503718.
[15] Ceclu L, Oana-Viorela N. Red beetroot: Composition and health effects - a review. J Nutr Med Diet Care. 2020;6:043.
[16] Mitchell MJ, Billingsley MM, Haley RM, Wechsler ME, Peppas NA, Langer R. Engineering precision nanoparticles for drug delivery. Nat Rev Drug Discov. 2021;20:101–24. doi: 10.1038/s41573-020-0090-8.
[17] Bolhassani A, Javanzad S, Saleh T, Hashemi M, Aghasadeghi MR, Sadat SM. Polymeric nanoparticles: potent vectors for vaccine delivery targeting cancer and infectious diseases. Hum Vaccin Immunother. 2014;10(2):321–32. doi: 10.4161/hv.26796, Epub 2013 Oct 15 PMID: 24128651; PMCID: PMC4185908.
[18] Civiale C, Licciardi M, Cavallaro G, Giammona G, Mazzone MG. Polyhydroxyethylaspartamide-based micelles for ocular drug delivery. Int J Pharm. 2009 Aug;378(1–2):177–86. doi: 10.1016/j.ijpharm.2009.05.028, Epub 2009 May 22 PMID: 19465101.
[19] Abuelsamen A, Mahmud S, Mohd Kaus NH, Farhat OF, Mohammad SM, Al-Suede FSR, et al. Novel Pluronic F-127-coated ZnO nanoparticles: Synthesis, characterization, and their in-vitro cytotoxicity evaluation. Polym Adv Technol. 2021;32(6):2541–51.
[20] Fusco S, Borzacchiello A, Netti PA. Perspectives on: PEO-PPO-PEO triblock copolymers and their biomedical applications. J Bioact Compat Polym. 2006;21(2):149–64.
[21] Elderdery AY, Alzahrani B, Hamza SMA, Mostafa-Hedeab G, Mok PL, Subbiah SK. Synthesis, characterization, and antiproliferative effect of CuO-TiO2-chitosan-amygdalin nanocomposites in human leukemic MOLT4 Cells. Bioinorg Chem Appl. 2022 Sep;2022:1473922. doi: 10.1155/2022/1473922, PMID: 36199748; PMCID: PMC9529517.
[22] Sarathbabu S, Marimuthu SK, Ghatak S, Vidyalakshmi S, Gurusubramanian G, Ghosh SK, et al. Induction of apoptosis by pierisin-6 in HPV positive HeLa and HepG2 cancer cells is mediated by the caspase-3 dependent mitochondrial pathway. Anticancer Agents Med Chem. 2019;19(3):337–46. doi: 10.2174/1871520619666181127113848, PMID: 30479220.
[23] Burganov TI, Katsyuba SA, Zagidullin AA, Zvereva EE, Miluykov VA, Sinyashin OG. Conjugation effects and optical spectra of 1,2-diphosphole cycloadducts. Russ Chem Bull. 2015;64:1896–900. doi: 10.1007/s11172-015-1090-4.
[24] Rahman MM, Khan SB, Jamal A, Faisal M, Aisiri AM. Iron oxide nanoparticles. Nanomaterials. 2011;3:43–67.
[25] Alagiri M, Hamid SBA. Green synthesis of α- Fe_2O_3 nanoparticles for photocatalytic application. J Mater Sci Mater Electron. 2014;25(8):3572–7.
[26] Bhuiyan MSH, Miah MY, Paul SC, Aka TD, Saha O, Rahaman MM, et al. Green synthesis of iron oxide nanoparticle using Carica papaya leaf extract: application for photocatalytic degradation of remazol yellow RR dye and antibacterial activity. Heliyon. 2020;6(8):e04603.
[27] Yardily A, Sunitha N. Green synthesis of iron nanoparticles using hibiscus leaf extract, characterization, antimicrobial activity. Int J Sci Res Revie. 2019;8(7).
[28] Haiss W, Thanh NT, Aveyard J, Fernig DG. Determination of size and concentration of gold nanoparticles from UV− Vis spectra. Anal Chem. 2007;79(11):4215–21.
[29] Demirezen DA, Yilmaz D, Yılmaz Ş. Green synthesis and characterization of iron nanoparticles using Aesculus hippocastanum seed extract. Int J Adv Sci Eng Technol. 2018;6:2321–8991.
[30] Pottker WE, Ono R, Cobos MA, Hernando A, Araujo JF, Bruno AC, et al. Influence of order-disorder effects on the magnetic and optical properties of $NiFe_2O_4$ nanoparticles. Ceram Int. 2018;44(14):17290–7.
[31] Zhang L, Yin L, Wang C, Lun N, Qi Y, Xiang D. Origin of visible photoluminescence of ZnO quantum dots: defect-dependent and size-dependent. J Phys Chem C. 2010;114(21):9651–8.
[32] Oliveira LH, De Moura AP, La Porta FA, Nogueira IC, Aguiar EC, Sequinel T, et al. Influence of Cu-doping on the structural and optical properties of CaTiO3 powders. Mater Res Bull. 2016;81:1–9.
[33] Bibi I, Kamal S, Ahmed A, Iqbal M, Nouren S, Jilani K, et al. Nickel nanoparticle synthesis using Camellia Sinensis as reducing and capping agent: Growth mechanism and photo-catalytic activity evaluation. Int J Biol Macromol. 2017;103:783–90.
[34] Rufus A, Sreeju N, Philip D. Synthesis of biogenic hematite (α-Fe_2O_3) nanoparticles for antibacterial and nanofluid applications. RSC Adv. 2016;6(96):94206–17.
[35] Nazar N, Bibi I, Kamal S, Iqbal M, Nouren S, Jilani K, et al. Cu nanoparticles synthesis using biological molecule of P. granatum seeds extract as reducing and capping agent: Growth mechanism and photo-catalytic activity. Int J Biol Macromol. 2018;106:1203–10.
[36] Ahmmad B, Leonard K, Islam MS, Kurawaki J, Muruganandham M, Ohkubo T, et al. Green synthesis of mesoporous hematite (α-Fe_2O_3) nanoparticles and their photocatalytic activity. Adv Powder Technol. 2013;24(1):160–7.
[37] Vihodceva S, Šutka A, Sihtmäe M, Rosenberg M, Otsus M, Kurvet I, et al. Antibacterial activity of positively and negatively charged hematite (α-Fe_2O_3) nanoparticles to escherichia coli, staphylococcus aureus and vibrio fischeri. Nanomaterials (Basel). 2021 Mar;11(3):652. doi: 10.3390/nano11030652. PMID: 33800165; PMCID: PMC7999532.
[38] Kombaiah K, Vijaya JJ, Kennedy LJ, Bououdina M, Ramalingam RJ, Al-Lohedan HA. Okra extract-assisted green synthesis of CoFe2O4 nanoparticles and their optical, magnetic, and antimicrobial properties. Mater Chem Phys. 2018;204:410–9.
[39] Zovko Koncić M, Kremer D, Karlović K, Kosalec I. Evaluation of antioxidant activities and phenolic content of Berberis vulgaris L. and Berberis croatica Horvat. Food Chem Toxicol. 2010 Aug–Sep;48(8–9):2176–80. doi: 10.1016/j.fct.2010.05.025, Epub 2010 May 17 PMID: 20488218.
[40] Mat Yusuf SNA, Che Mood CNA, Ahmad NH, Sandai D, Lee CK, Lim V. Optimization of biogenic synthesis of silver nanoparticles from flavonoid-rich Clinacanthus nutans leaf and stem aqueous extracts. R Soc Open Sci. 2020 Jul;7(7):200065. doi: 10.1098/rsos.200065. PMID: 32874618; PMCID: PMC7428249.
[41] Pandey KB, Rizvi SI. Plant polyphenols as dietary antioxidants in human health and disease. Oxid Med Cell Longev. 2009 Nov–Dec;2(5):270–8. doi: 10.4161/oxim.2.5.9498, PMID: 20716914; PMCID: PMC2835915.
[42] Rehana D, Mahendiran D, Kumar RS, Rahiman AK. Evaluation of antioxidant and anticancer activity of copper oxide nanoparticles synthesized using medicinally important plant extracts. Biomed Pharmacother. 2017;89:1067–77.
[43] Abdal Dayem A, Hossain MK, Lee SB, Kim K, Saha SK, Yang GM, et al. The role of Reactive Oxygen Species (ROS) in the biological activities of metallic nanoparticles. Int J Mol Sci. 2017 Jan;18(1):120. doi: 10.3390/ijms18010120, PMID: 28075405; PMCID: PMC5297754.

[44] Manke A, Wang L, Rojanasakul Y. Mechanisms of nanoparticle-induced oxidative stress and toxicity. Biomed Res Int. 2013;2013:942916. doi: 10.1155/2013/942916 Epub 2013 Aug 20. PMID: 24027766; PMCID: PMC3762079.

[45] Alarifi S, Ali D, Alkahtani S, Alhader MS. Iron oxide nanoparticles induce oxidative stress, DNA damage, and caspase activation in the human breast cancer cell line. Biol Trace Elem Res. 2014;159(1):416–24.

[46] Govindarajan M, Nicoletti M, Benelli G. Bio-physical characterization of poly-dispersed silver nanocrystals fabricated using carissa spinarum: A potent tool against mosquito vectors. J Clust Sci. 2016;27:745–61. doi: 10.1007/s10876-016-0977-z.

[47] Karthika V, AlSalhi MS, Devanesan S, Gopinath K, Arumugam A, Govindarajan M, et al. Chitosan overlaid Fe_3O_4/rGO nanocomposite for targeted drug delivery, imaging, and biomedical applications. Sci Rep. 2020;10:18912. doi: 10.1038/s41598-020-76015-3.